Simulation of Ramp Compression Using Finite Volume Schemes

Riley Jacobs

April 28, 2023

Abstract

This final term project investigates the effects of ramp angles and varying supersonic mach numbers for a compression ramp, particularly with respect to its treatment of oblique shocks. The study employs a numerical approach utilizing the finite volume method, with Godunov's method and Roe's approximate Riemann solver, as well as the Harten-Lax-van Leer-Einfeldt (HLLE) scheme to approximate the numerical fluxes (superposition of Riemann problems) to solve the 2-D compressible, inviscid Euler equations. Then the results will be compared to analytical, experimental and other numerical data available in literature.

1 Introduction of the Problem

Over the past century, the ramp compression problem has been extensively studied through experimental, analytical, and numerical methods, owing to its simple geometry and easily defined boundary conditions. When a supersonic flow encounters an inclined surface, it changes direction to meet the solid boundary condition, resulting in flow compression and the formation of an oblique shock. This phenomenon is commonly observed in ramp-like or wedge-like structures. For this project, I will consider a rectangular channel with a significantly larger depth than height, allowing for the flow to be modeled as two-dimensional. The objective of this project is to solve the steady, inviscid and compressible Navier-Stokes equations for a flow through a rectangular domain with varying ramp sizes. Figure 1, illustrates the geometry of the problem, including the necessary boundary conditions to achieve a steady-state solution. All flows investigated in this project will be supersonic, with the entrance to the domain considered as uniform flow velocity.

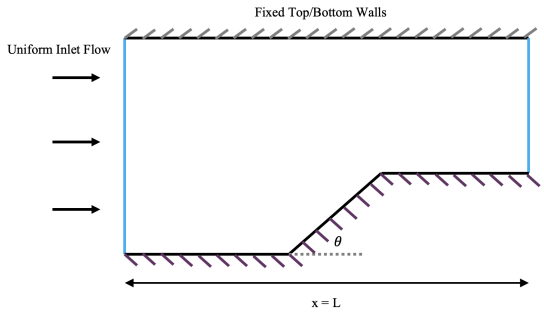

Figure 1: Supersonic Ramp Compression.

The results obtained through numerical simulation will be validated against the literature, experimental results and the analytical solution based on oblique shock theory.

2 Literature Review

The Navier-Stokes analysis of a supersonic flow over a compression ramp is a topic of special interest in the field of fluid mechanics and aerospace engineering. The study aims to analyze the behavior of a supersonic flow over a 2D wedge or ramp, which is an important component in many aerospace applications, such as supersonic engine inlets and outer body of missiles.

In one study, the schemes of ROE, HLLC, HLLC+, HLLE+, and HLLE++ were all implemented for an inviscid $M_\infty = 4$ flow over a two-dimensional 30 degree wedge [1]. Utilizing a van Albada flux limiter, it was shown that for the same number of iterations on both a medium and fine grid that HLLE++ produced the least density oscillation. That being said, HLLE+, HLLE++ and HLLC+ all provided accurate density behind the shock based on theoretical understanding. The Roe algorithm convergence improves with increasing discretization, but remains relatively error prone.

DeBonis et al. (2019) compiled eight numerical studies for a $M_\infty = 2$ flow over a 15 degree wedge using both structured and unstructured solvers [2]. They tested various combinations of spatial operators and flux limiters and investigated the Roe second and HLLE second methods with minmod limiters. Some small differences between the cases were seen up close to the region near the shock wave, and all solutions were relatively similar, except for the structured solver's Roe scheme, which produced a stronger post-shock oscillation.

In another study, Kolesnik, & Smirnov implemented an inviscid supersonic flow in a duct with a central wedge [3]. They assumed an inlet Mach number of $M_\infty = 3$ and achieved second-order spatial discretization using the MUSCL approach. They also extended their research to include implementing the Roe linearization scheme for comparison. They found that wall pressure breakdown occured in both schemes and this effect can be suppressed by introducing a limiter in combination.

Beyond the scope of this project, Chen et al. (2019) [8] conducted a numerical study of a supersonic flow over a compression ramp with different ramp motion modes, including ramp oscillation and ramp rotation. They used a high-order numerical method to solve the Navier-Stokes equations for a Mach 3 flow over a compression ramp. They found that the ramp motion had a significant effect on the flow field and the shock wave structure, and

the ramp rotation mode was more effective in reducing the drag coefficient compared to the ramp oscillation mode.

In conclusion, various numerical methods have been employed to investigate shock compression interaction in supersonic flows, with the ultimate goal of understanding the behavior of the flow field and optimizing the design of aerospace components.

3 Governing Equations of Fluid Dynamics

Euler Inviscid Equations

For high speed flow, in the regime of supersonic and hypersonic flow, the flow is considered inviscid. Therefore, the Navier-Stokes equations can be simplified by neglecting the viscosity term ($\mu = 0$) and thermal conductivity term ($k = 0$). This simplification results in the Euler equations, which describe the motion of high speed flows. In two dimensions, the non-linear hyperbolic Euler equations can be written as:

$$\frac{\partial \rho}{\partial t} + \nabla \cdot (\rho \underline{u}) = 0$$

$$\frac{\partial \rho}{\partial t} + \nabla \cdot (\rho \underline{u} \otimes \underline{u}) = -\nabla P + \rho \underline{b}$$

$$\frac{\partial \rho E}{\partial t} + \nabla \cdot (\rho \underline{u} H) = \rho \underline{b} \cdot \underline{u} + s$$

Without body forces or heat addition, the Euler equations can be rewritten as:

$$\frac{\partial \rho}{\partial t} + \nabla \cdot (\rho \underline{u}) = 0 \tag{1}$$

$$\frac{\partial \rho}{\partial t} + \nabla \cdot (\rho \underline{u} \otimes \underline{u}) = -\nabla P \tag{2}$$

$$\frac{\partial \rho E}{\partial t} + \nabla \cdot (\rho \underline{u} H) = 0 \tag{3}$$

To compile the equations, define the state vector $\mathbf{U} = \mathbf{U}(x, y, t)$, the flux vector $\mathbf{F} = \mathbf{F}(\mathbf{U})$ in the x direction and the flux vector $\mathbf{G} = \mathbf{G}(\mathbf{U})$ in the y direction. Once again, define enthalpy (H) so enthalpy can be rewritten as $H = E + \frac{P}{\rho}$. Then the two-dimensional, unsteady Euler equations read

$$\frac{\partial \mathbf{U}}{\partial t} + \frac{\partial \mathbf{F}}{\partial x} + \frac{\partial \mathbf{G}}{\partial y} = 0$$

this means

$$\mathbf{U} = \begin{bmatrix} \rho \\ \rho u \\ \rho v \\ E \end{bmatrix}, \mathbf{F} = \begin{bmatrix} \rho u \\ \rho u^2 + p \\ \rho uv \\ u(E + p) \end{bmatrix}, \mathbf{G} = \begin{bmatrix} \rho v \\ \rho uv \\ \rho v^2 + P \\ v(E + p) \end{bmatrix}$$

combining into one flux vector

$$\vec{F} = F_x + F_y = \begin{bmatrix} \rho u \\ \rho u^2 + p \\ \rho uv \\ u(E+p) \end{bmatrix} \frac{\partial}{\partial x} + \begin{bmatrix} \rho v \\ \rho uv \\ \rho v^2 + P \\ v(E+p) \end{bmatrix} \frac{\partial}{\partial y}$$

where $\rho([\frac{m^3}{g}])$ is the density, $\rho u([\frac{kg}{m^2 s^1}])$ and $\rho v([\frac{kg}{m^2 s^1}])$ are the x and y components of the fluids momentum per unit volume, P ($[\frac{N}{m^2}]$) is the pressure and E ($[\frac{j}{m^3}]$) is the total energy per unit volume. This means we have five equations (1 vector, 2 scalar) and six unknowns ρ, u, v, P, E, H. The following equations are then required for closure of the Euler equations and implementation in numerical simulation.

$$E = \rho(\frac{|\mathbf{u}|^2}{2} + e) = \rho(\frac{|\mathbf{u}|^2}{2} + C_v T) \tag{4}$$

$$|\mathbf{u}|^2 = (u^2 + v^2)/2 \tag{5}$$

$$p = \rho RT = (\gamma - 1)\rho e = (\gamma - 1)(E - \rho|\mathbf{u}|^2/2) \tag{6}$$

Despite their simplicity, the unsteady Euler equations enable us to exhibit the key behaviors of compressible fluids at high Mach numbers such as the formation of shocks.

4 Chosen Numerical Scheme

4.1 Finite Volume Method

The literature review highlights that most compressible Euler equation solvers use structured grids to solve the Navier-Stokes equations with the finite volume method. In this method, the advective terms are solved using the popular Godunov-type (upwind) method, where the inter-cell numerical fluxes are calculated by solving the Riemann problems using reconstructed values of the conserved variables at the cell interfaces. It has been found that finite volume schemes are better than flux splitting approaches due to their superior resolution of discontinuities [5]. Thus, I have chosen to implement the superior finite volume method to simulate my ramp compression problem. The finite volume method in integral form can be shown by

$$\frac{\mathrm{d}}{\mathrm{d}t} \oint_{\Omega(t)} \mathbf{U}\, dV = \oint_{\Omega(t)} \frac{\partial \mathbf{U}}{\partial t}\, dV + \oint_{\partial\Omega(t)} (\underline{u} \cdot \mathbf{n})\mathbf{U}\, dA$$

With simplifying assumptions of inviscid and 2D, the Euler equations are expressed as

$$\frac{\partial}{\partial t} \oint_{\partial\Omega(t)} \mathbf{U}\, dA + \oint_{L} (\mathbf{F}\hat{i} + \mathbf{G}\hat{j}) \cdot \mathbf{n}\, dl = 0$$

where $\partial\Omega(t)$ is the area of the control surface, L is the length of the control surface boundary, F and G are the flux tensors of the x and y directions respectively, and $\mathbf{n}$ is the unit normal vector to the control surface.

$$\frac{\partial}{\partial t}\oint_{\partial\Omega(t)} \mathbf{U}\,dxdy + \oint_L (\mathbf{F}\hat{i} + \mathbf{G}\hat{j})\cdot\mathbf{n}\,dl = 0$$

The solution is then advanced in time using an explicit upwind forward Euler method due to its simplicity and ease of numerical implementation.

Godunov Scheme

In his 1959 paper, Godunov [6] outlined his first order finite volume method. It can be described as follows:

$$u_i^{n+1} = u_i^n - \frac{h}{\Delta x}(f^n_{i+\frac{1}{2}} - f^n_{i+-\frac{1}{2}})$$

where u_i^n is defined as:

$$u_i^n = \frac{1}{\Delta x}\int_{x_{i-1}}^{x_{i+1}} U(x, nh)\,dx$$

and $f^n_{i+\frac{1}{2}}$ is defined as:

$$F^n_{i+\frac{1}{2}} = \frac{1}{\Delta t}\int_{t_n}^{t_{n+1}} f(U(x_{i=1/2}, t))\,dt$$

Godunov observed that at each cell interface the numerical flux can be described as a Riemann problem. This means that the Riemann problem at every time can be solved explicitly in terms of waves, emanating from each interface. This form is the standard form of a finite volume scheme and can be solved explicitly for the scalar Euler conservation laws.

Linearized Riemann Solvers

Roe Scheme

In order to use the Godunov scheme, I will begin by replacing the exact solutions of the Riemann problem with two approximate Riemann solvers. The first solver is Roe, which linearizes the nonlinear equations. The finite volume scheme with a Roe flux is implemented by the following formula:

$$F^n_{i+\frac{1}{2}} = F^{Roe}(U^n_i, U^n_{i+1}) = \begin{cases} f(U^n_j) & A_{j+1/2} \geq 0 \\ f(U^n_{j+1}) & A_{j+1/2} \leq 0 \end{cases}$$

In order to improve Roe, Harten's entropy fix is often employed. In Harten's entropy fix, the eigenvalues λ_i in Roe's scheme are modified as:

$$\lambda_i = \begin{cases} \frac{\lambda_i^2+\delta^2}{2\delta} & |\lambda_i| \leq \delta \\ |\lambda_i| & |\lambda_i| \geq \delta \end{cases}$$

where $\delta = \delta_0(|u|+a)$ and δ_0 is a constant parameter. For this type of problem, $\delta_0 = \frac{1}{5}$ is often used. This particular linearized solver fails at resolving rarefractions, but as my particular problem consists of a single wave traveling to the right (or to the left depending on the sign of A), the Roe scheme should be sufficient to capture the shock phenomena present in the

problem [7].

HLLE Scheme

I will additionally implement the Harten-Lax-van Leer-Einfeldt (HLLE) flux function method as it is rather simple and efficient. This particular scheme keeps only the largest and smallest characteristics and averages intermediate states in-between.

$$\vec{U}_{HLLE} = \begin{cases} f(U_j^n) & S_L \geq 0 \\ f(U^*) & S_L \leq 0 \leq S_R \\ f(U_{j+1}^n) & S_R \leq 0 \end{cases}$$

where $\vec{U^*}$ is defined as

$$\vec{U^*} = \frac{S_L(U_{i+1}^n) - S_L(U_i^n) - (\underline{F_R} - \underline{F_L})}{S_R - S_L}$$

making the flux for the HLLE scheme computed as follows:

$$F_{i+\frac{1}{2}}^n = F^{HLLE}(U_i^n, U_{i+1}^n) = \frac{S^+F(U_i^n) - S^-F(U_{i+1}^n)}{S^+ - S^-} + \frac{S^+S^-}{S^+S^-}(U_{i+1}^n - U_i^n)$$

Additional constraints such as the CFL condition is key to ensure the stability of the numerical solver [7]. This is taken by the form of:

$$CFL = \frac{c\Delta t}{\Delta x} \leq 1$$

where c is the maximum wave speed. Depending on the implementation of Roe or HLLE the maximum wave speed is defined differently, but it remains key to ensuring that the solver remains stable and that the solver will eventually converge to a steady state.

4.2 Boundary Conditions

The boundary conditions for the velocity field are relatively straightforward. There are three kinds of boundaries to be defined in this problem: inlet, exit, and the wall or a solid wall boundary. At the inlet, a uniform velocity in the x-direction is enforced, while the top and bottom boundary velocities have a no-penetration condition imposed on them. This means that the velocity vector component normal to the surface is set to zero to satisfy the no-through boundary conditions. The solid walls are numerically enumerated as frictionless walls to generate fluxes mirroring the normal flux of border cells into the wall. Mathematically and numerically this is imposed by:

$$n_x u = n_y v = 0$$

Substituting this expression into our Euler equations, it can be easily satisfied by,

$$\vec{n}\vec{F} = \begin{bmatrix} n_x(\rho u) + n_y(\rho v) \\ n_x(\rho u^2 + p) + n_y(\rho uv) \\ n_x(\rho uv) + n_y(\rho v^2 + p) \\ n_x(u(E+p)) + n_y(v(E+p)) \end{bmatrix} = \begin{bmatrix} 0 \\ n_x p \\ n_y p \\ 0 \end{bmatrix}$$

Unlike incompressible flow, there is no need to solve Poisson's equation for pressure, but we only need to account for pressure using the state equation. As discussed in lecture, under finite volume convention the cell state is located at the volume centroid of each cell. In summary, the "wind tunnel" will contain a uniform flow in the x-direction with density $\rho = 1$, pressure $P = 1.4$, and will be investigated at both Mach 2 and 3 with varying ramp sizes.

4.3 Grid and Mesh Structure

A refined mesh was generated in Matlab to simulate the flow over a ramp, which is commonly found on high-speed vehicle surfaces or inlets to engines. The mesh was divided into three major regions: pre-shock, ramp, and post-shock. The mesh refinement process was carried out to ensure that the mesh is accurately refined for visualizing and analyzing the development of the oblique shock at the base of the ramp. As we begin to define parameters within our mesh, it was important that the nodes, vertices, unit normals and lengths in the x and y direction of each of our control volumes were catalogued. To do this, I critically calculated the length of the each edge using the following formula.

$$\Delta s = \sqrt{\Delta x^2 + \Delta y^2}$$

This process took great care as it can be somewhat tedious to be smart during the "bookkeeping" process in creating a new mesh. The first refinement was to reduce the number of cells in the pre-shock region (as the flow will remain uniform) while increasing the number of cells in the post-shock region. This will provide the required resolution to capture the post-ramp behavior as the shock reflects of the top and bottom walls. Additionally, to capture the rapid changes in flow properties closer to the wall, a scaling or "stretching" has been applied in the y-direction, creating a greater number of cells closer to the wall. Finally, to further refine the mesh domain, each square control volume has been divided into two triangular control volumes. This process resulted in the mesh shown below.

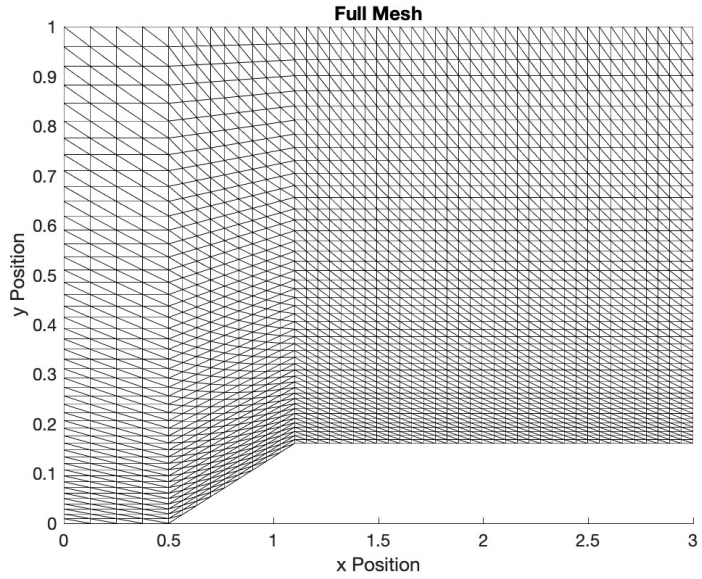

(a) "Rough" Mesh

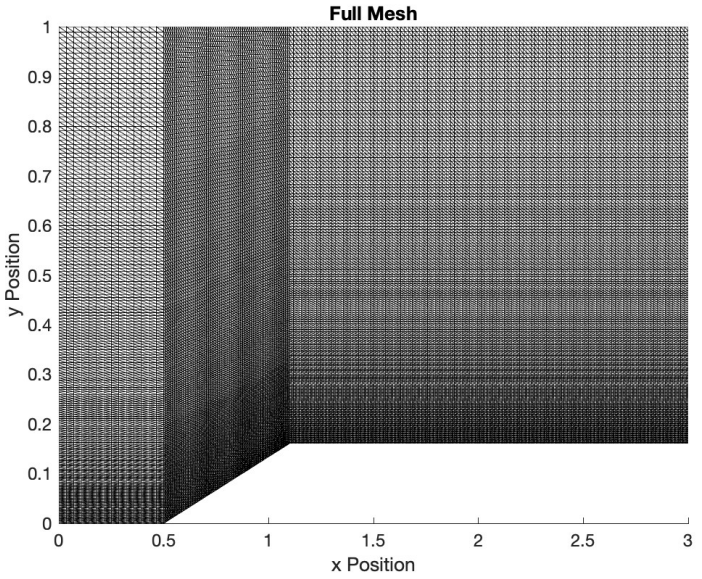

(b) "Fine" Mesh

Figure 2: Refinement of Mesh

A convergence study was conducted to evaluate the effect of increasing the number of control volumes on the simulation results. It was observed that as the number of control volumes increased, the characteristics of the flow became clearer and the "finer" details became easier to see. This can be attributed to the fact that a higher number of control volumes allows for a greater discretization of the flow domain and a better resolution of the flow features. The convergence study demonstrated that increasing the number of control volumes significantly improves the accuracy and reliability of the simulation results. Therefore, it is recommended to use a sufficiently large number of control volumes to ensure that the flow

characteristics are captured accurately and the simulation results are reliable. This is easily visualized in the figure below as it is clear the mach contours become more defined with more control volumes (both plots below were created using the HLLE solver).

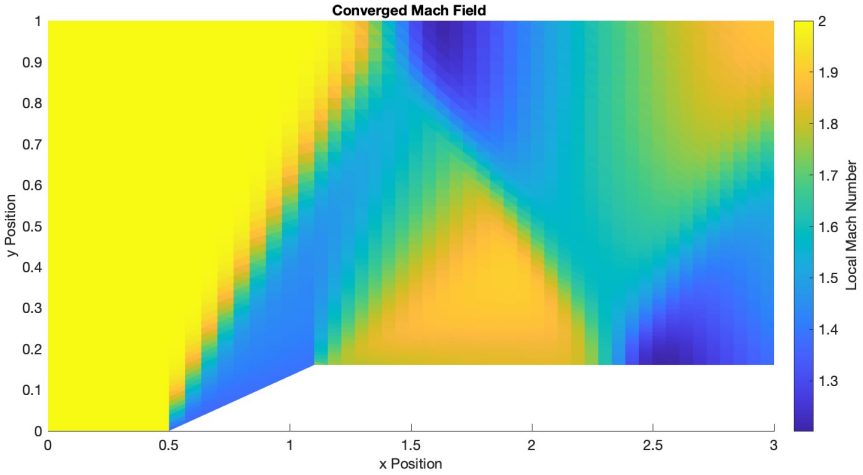

(a) Unrefined Mach Field for M = 2 and a $\theta = 15°$ wedge.

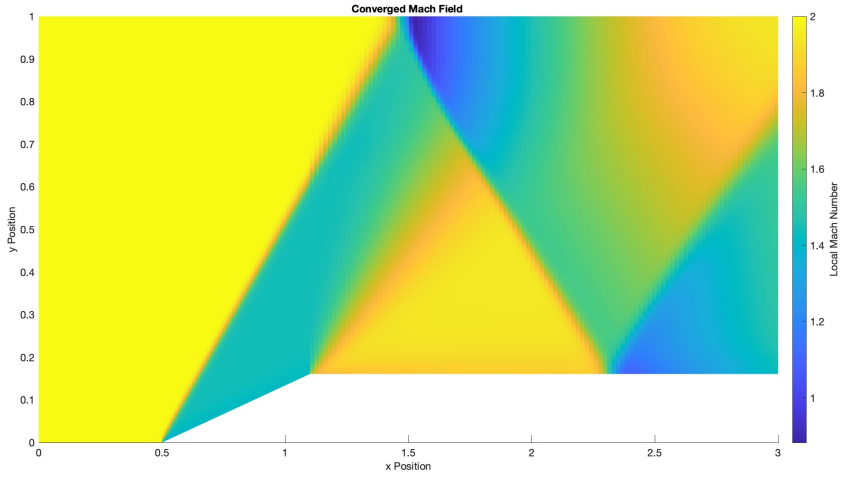

(b) Converged Mach Field for M = 2 and a $\theta = 15°$ wedge.

Figure 3: Converged Mach Contours for Roe vs HLLE

Therefore, the rest of my analysis was evaluated on the refined mesh for both the Roe and HLLE solver in the results section.

4.4 Formulation of the Computer Code

The finite volume method with Roe and HLLE linearization Riemann schemes was implemented to integrate the Euler equations in Matlab. First, the mesh was formulated by creating triangular control volumes across the domain based on discretization parameters (worthy of note, the same discretization node points in the x and y). Then the initial, inlet

boundary and exit boundary conditions were imposed in the form of the conserved variables. At each time step, the solver is used to calculate the fluxes (i.e., the rates of mass, momentum, and energy flow) at each point in a computational grid, based on the state of the fluid at that point. Then in order to impose the solid wall boundary conditions, boundary nodes were specified and boundary conditions were imposed along those boundary nodes (depending on the boundary). The inlet and exit boundary conditions were then reimposed at the end of each time step. The following algorithm was used to build my Roe solver. It is important to note that before applying the scheme, the entropy fix was employed in my Roe scheme, but not explicitly outlined in the algorithm below.

Roe Algorithm

1. Compute the Roe average values, $\tilde{p}, \tilde{u}, \tilde{v}, \tilde{H}$ and $\tilde{a}$
2. Compute the eigenvalues λ_i and evaluating them on the averages
3. Compute the right eigenvectors and wave strengths evaluated on the averages
4. Use all the above quantities to compute $F_{i+\frac{1}{2}}$
5. Compute the Roe flux as $F_n = \frac{1}{2}(F_{nL} + F_{nR}) - \frac{1}{2}\sum_{i=1}^{4} \lambda_i(ws_i R_i))$
6. Then we know that the max domain for a Roe solver will be $|\tilde{u}|$

Note: A similar algorithm was also developed for my HLLE solver and employed using Matlab.

5 Results and Discussion

5.1 Results

The results obtained from my study showed a striking similarity to what is to be expected from theoretical understanding of shock behavior over a compression ramp. The following Mach contours paint a coherent picture that aligns well with our literature review. The figures below depict the differences between the two solvers, Roe and HLLE, respectively. It is immediately apparent that although both solvers exhibit overall trends in pressure and Mach numbers across the major shocks and expansion fans, there are some stark differences between the two converged solver solutions.

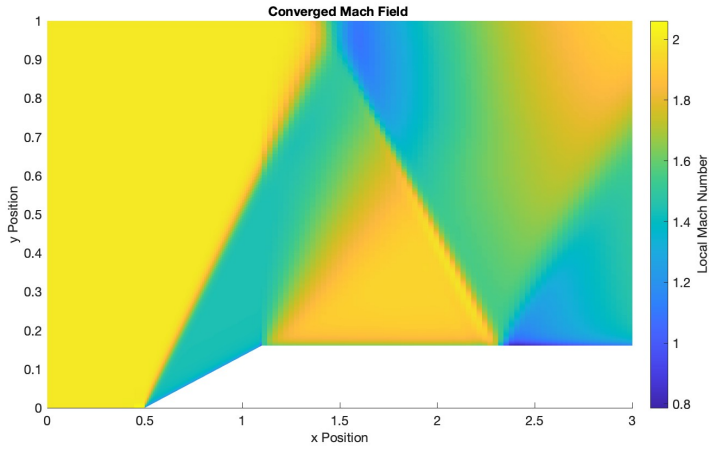

(a) Converged Roe Case

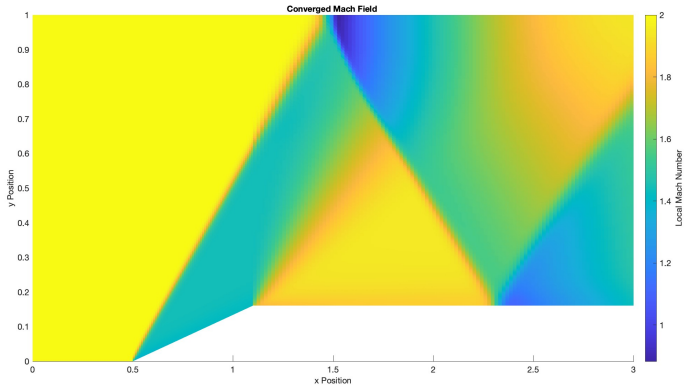

(b) Converged HLLE Case

Figure 4: Converged Mach Contours for Roe vs HLLE

Visually, it is apparent that the HLLE solver exhibits an oblique shock that is located further aft of the ramp. This is confirmed computationally, as the Roe figure yields an oblique shock of $\beta \approx 46$ while the HLLE solver yields a value of $\beta \approx 45$. These results suggest that the HLLE solver more closely aligns with our theoretical expectations. This is further supported by the pressure trends observed following the oblique shock, as shown in the figure below.

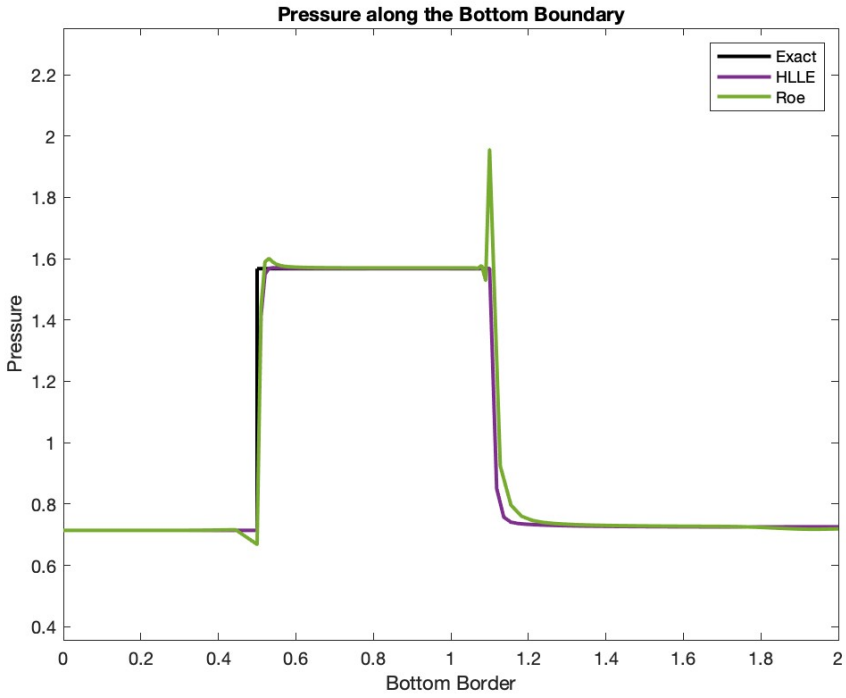

Figure 5: Converged Mach Field for M = 2 and a $\theta = 15°$ wedge.

While both solvers exhibited the anticipated pressure ratio of 2.19 across the oblique shock, the Roe solver demonstrates abrupt pressure fluctuations along the domain that were absent in the HLLE solver. These spikes were prominently visible as the Roe solver had inadequate resolution along the ramp. Moreover, higher Mach numbers were observed near the bottom wall, indicating a deviation from the expected values. These lower mach numbers along the boundary or bottom of the ramp are highlighted in the unrefined mesh and extracted mach values along the bottom boundary for the Roe solver below.

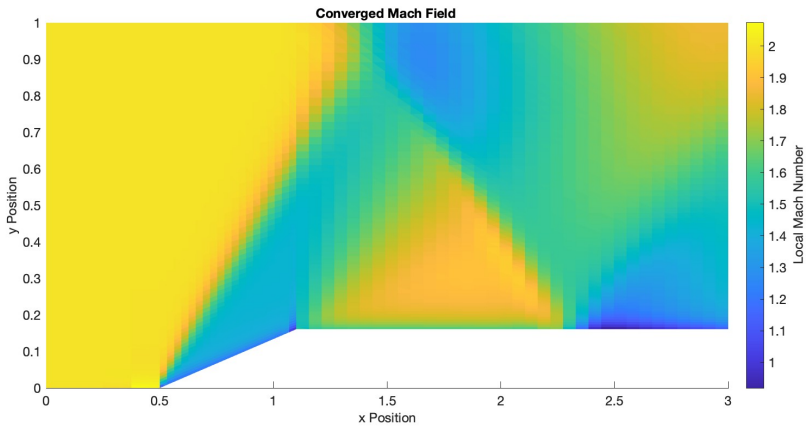

(a) Mach Contour

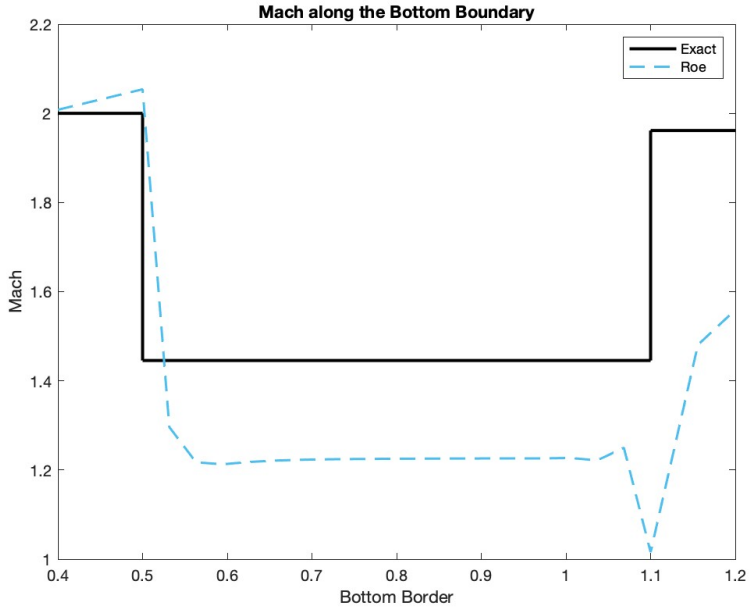

(b) Extracted Mach Values

Figure 6: Unrefined Mach Field for M = 2 and a $\theta = 15°$ wedge using Roe Solver

It is even more obvious from the outlined figures above that Roe severely diverges from post-shock calculations close to the wall. All these observations substantiate the argument that Roe is a competent numerical solver, but HLLE is a more reliable choice, particularly in areas with significant discontinuities. This is primarily due to HLLE being positively conservative when the absolute values of the maximum and minimum wave speeds meet the CFL stability constraints. Thus, the following figures demonstrate the "final" HLLE converged mach contours and pressure contours for $M_\infty = 2$ and a $\theta = 15°$.

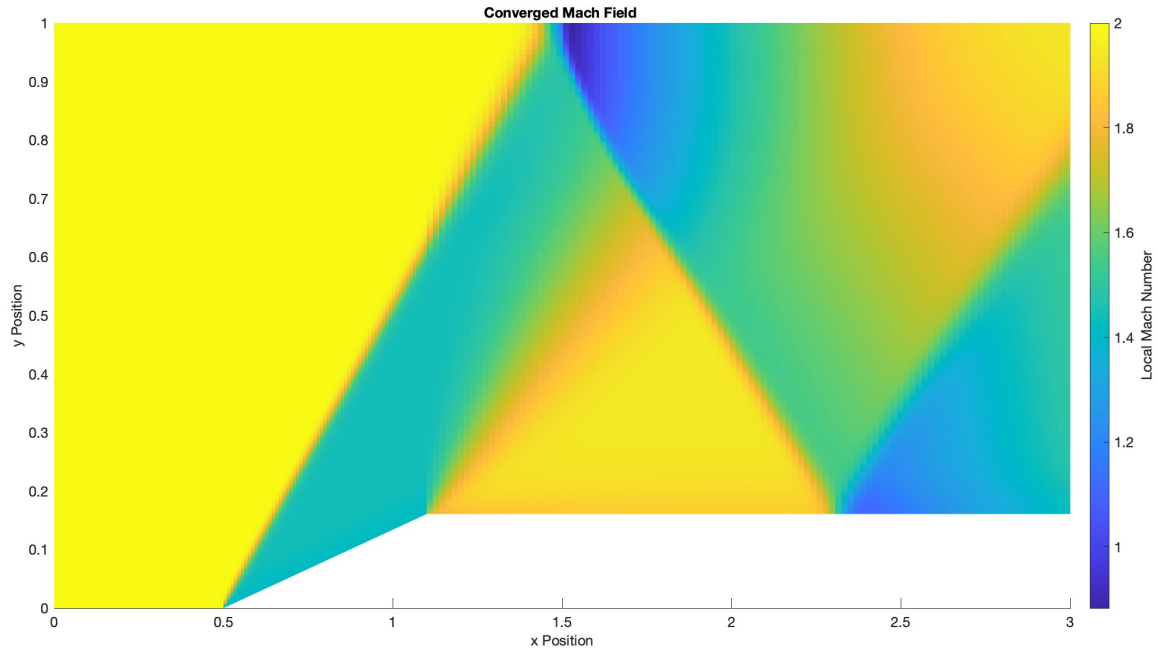

Figure 7: Converged Mach Field for M = 2 and a $\theta = 15°$ wedge.

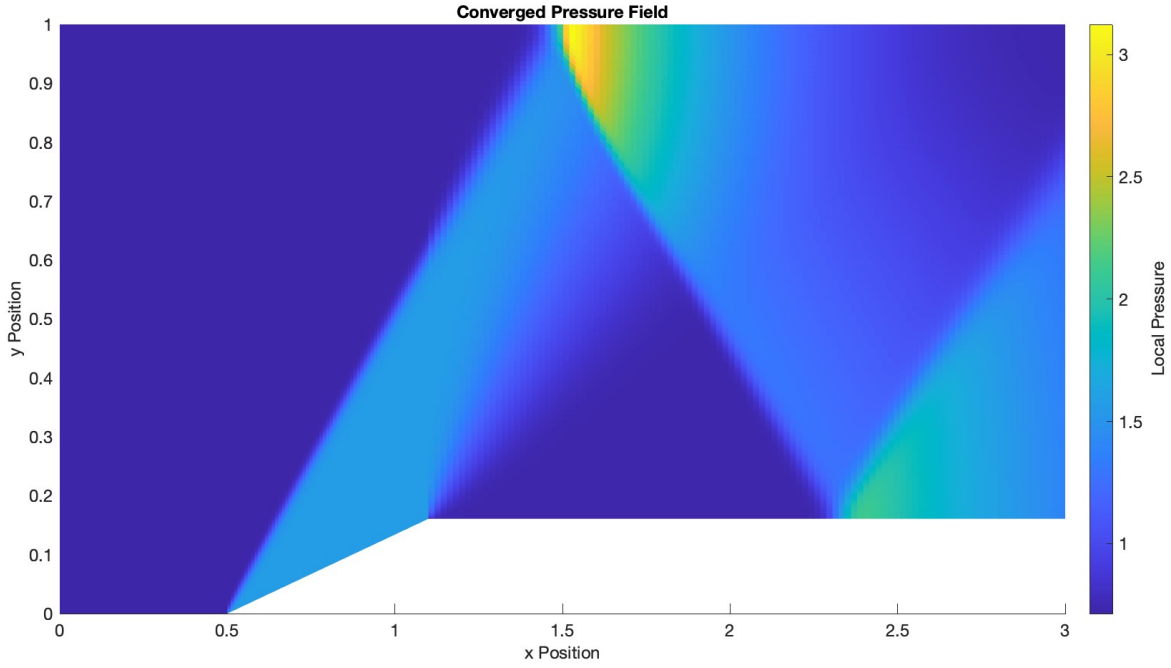

Figure 8: Converged Pressure Field for M = 2 and a $\theta = 15°$ wedge.

All of these results provide the argument that when comparing my numerical solvers

performance to theoretical understanding, the HLLE scheme will be chosen over Roe as my numerical scheme of choice.

6 Comparison to Literature Findings

6.1 Analytical comparison

Based on the results obtained from my CFD compressible flow solver, it can be concluded that it accurately simulated an oblique shock over a wedge. This is supported by the fact that the simulation results align well with the theoretical expectations for this type of flow. The solver's ability to capture the complex flow physics accurately indicates that it is well-suited to handle this type of problem. The analytical solution is plotted as the solid black "ramp" line in each of the following pressure figures. Therefore, it can be concluded that the simulation results are reliable and can be used to gain further insights into the flow characteristics of oblique shocks over wedges within real flow scenarios.

6.2 NASA release

In one study, the schemes of ROE, HLLC, HLLC+, HLLE+, and HLLE++ were all implemented for an inviscid $M_\infty = 2$ flow over a two-dimensional 15 degree wedge [1]. Utilizing a van Albada flux limiter, it was shown that for the same number of iterations on both a medium and fine grid that HLLE++ produced the least density oscillation. That being said, HLLE+, HLLE++ and HLLC+ all provided accurate density behind the shock based on theoretical understanding. The Roe algorithm convergence improves with increasing discretization, but remains relatively error prone.

In order to compare the NASA release with my own solver, I replicated the testing conditions with an inviscid $M_\infty = 2$ inlet flow over a two-dimensional 15 degree ramp. The results were then run with both Roe and HLLE. It is clear both visually as well as analytically using pressure ratio experienced across the shock that each solvers converged solution are virtually identical. Worthy of note, the solver of HLLE was chosen for both mach contour and HLLE as it provided faster convergence for higher mesh resolution than my Roe solver. The mach contour for the NASA release and my own solver are shown side by side below.

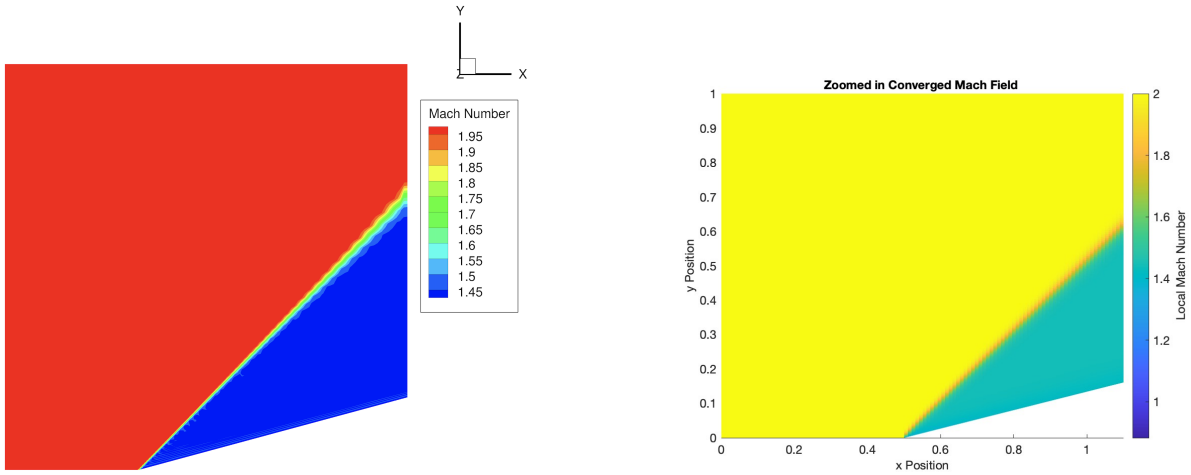

(a) NASA Validation Case

(b) Zoomed in wedge structure

Figure 9: Three simple graphs

The comparison between my simulation and the reference simulation reveals that both simulations match closely in terms of the pressure distribution experienced over the wedge as well as the Mach contours. This is clear because both solvers experienced a pressure ratio of 2.19 as well as an aft flow or post-shock flow of $M_2 = 1.44$. This close agreement between the two simulations further validates the accuracy of the results obtained from my simulation and the implementation of Roe and HLLE code. These numbers are similarly correlated and validated in which they are practically identical to what we know from oblique shock theory. This is shown in the pressure distribution below for each of the solvers.

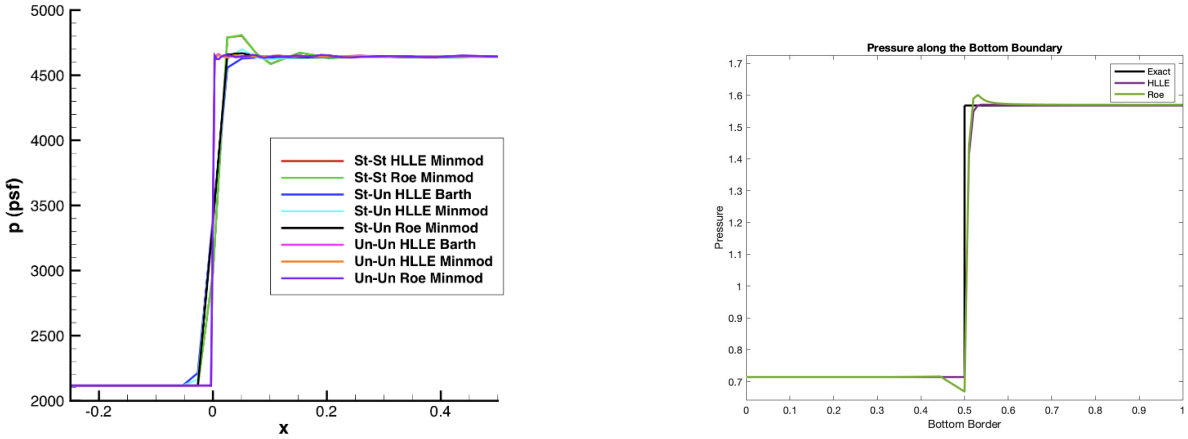

(a) NASA Validation Case

(b) Zoomed in wedge structure

Figure 10: Pressure Distributions my HLLE solver vs NASA

From figure 10, it is clear that the solver quickly responds to the presence of the ramp ($x = 0.5$) and immediately feels a drop in pressure as the flow instantaneously slows down

following the oblique shock. Both in the validation case as well as my own solvers solution, both of the Roe solvers demonstrated an overshooting behavior following the oblique shock. This is likely due to the fact that HLLE, as opposed to the Roe method, is a more robust method and could more accurately approximate the Riemann problem - especially in the absence of viscosity. Moreover, my solver suffers from a dip in pressure just prior to the ramp's start. This may be a consequence of not introducing a flux limiter (like the test case's use of minmod flux limiter). Flux limiters avoid the spurious oscillations that occur in numerical CFD solver and thus, future work may benefit from adding minmod limiters to smoothen out such curves in pressure jumps. The fact that my simulation has produced results that are consistent with the reference simulation indicates that my code is capable of accurately modeling the ramp compression. These findings provide additional confidence in both the study and the code developed, indicating that they can be used for further analysis and investigation of the flow behavior over similar geometries.

6.3 Kolesnik and Smirnov

In their study [3], Kolesnik and Smirnov simulated an inviscid supersonic flow in a duct featuring a central wedge. The authors considered an inlet Mach number of $M_\infty = 3$ and employed a second-order spatial discretization approach using the MUSCL method. They also investigated the implementation of the Roe linearization scheme to compare its performance. The study revealed that both schemes resulted in wall pressure breakdown, which could be mitigated by introducing a limiter in combination with the schemes.

In order to replicate and validate my solver with their results, I reconstructed my grid to reflect the two ramp angles that the flow experienced. It is quickly clear from visual inspection that we found similar behaviors of shock and wall interactions through the full "wind tunnel" domain. The following mach contours are compared to my own for an inviscid $M_\infty = 3$ inlet flow over a two-dimensional $\theta = 16.7°$ and $\theta = 30.9°$ ramp.

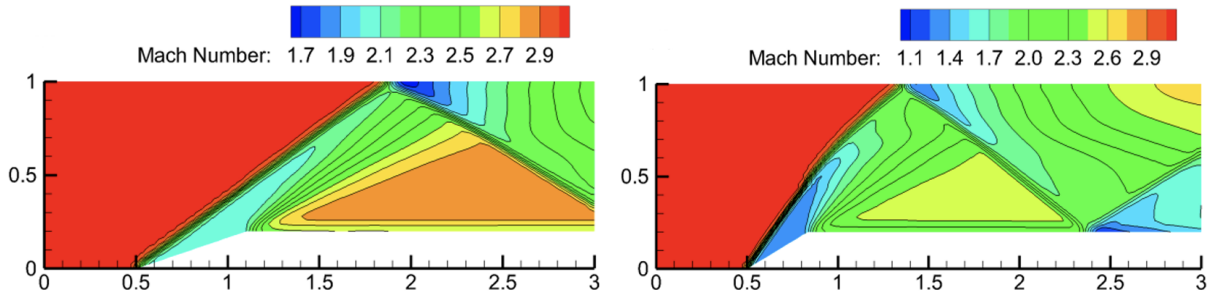

(a) M = 3 and a $\theta = 16.7°$ (b) M = 3 and a $\theta = 30.9°$

Figure 11: Kolesnik and Smirnov Fields of Mach number

In order to to replicate their wind tunnel domain and initial conditions, I reconstructed my mesh to vary my ramp length (rather than holding my ramp length steady) while holding the ramp's x-location starting point steady. The following Mach contours demonstrate the effect of such a ramp in my own numerical simulation (both using HLLE solver).

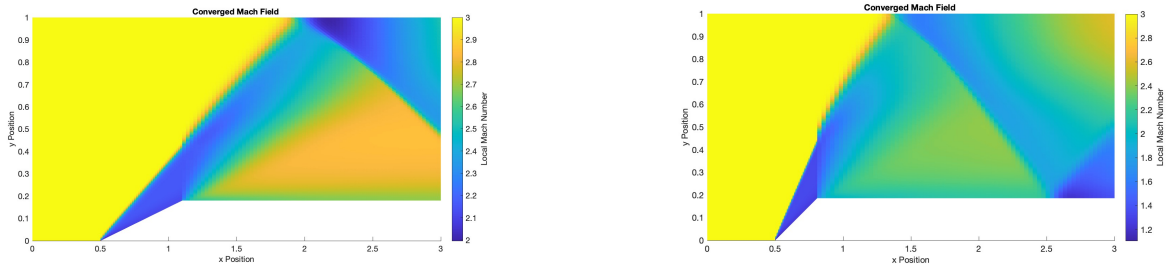

(a) M = 3 and a $\theta = 16.7°$ ramp

(b) M = 3 and a $\theta = 30.9°$ ramp

Figure 12: Pressure Distributions using my HLLE solver

Visual inspection indicates that both solutions adhere to the overarching trends, particularly when examining the shock reflections at the top boundaries. Further work would benefit from greater discretization in the post-shock region, however, the computational cost on my own local machine prevented me from greater resolution in that region. Nonetheless, both simulations were able to accurately match the post-shock Mach number and the pressure ratio along the shock of the ramp compression. The figure below outlines that Kolesnik and Smirnov's solver demonstrated a pressure ratio of 3.3 and 6.7, respectively.

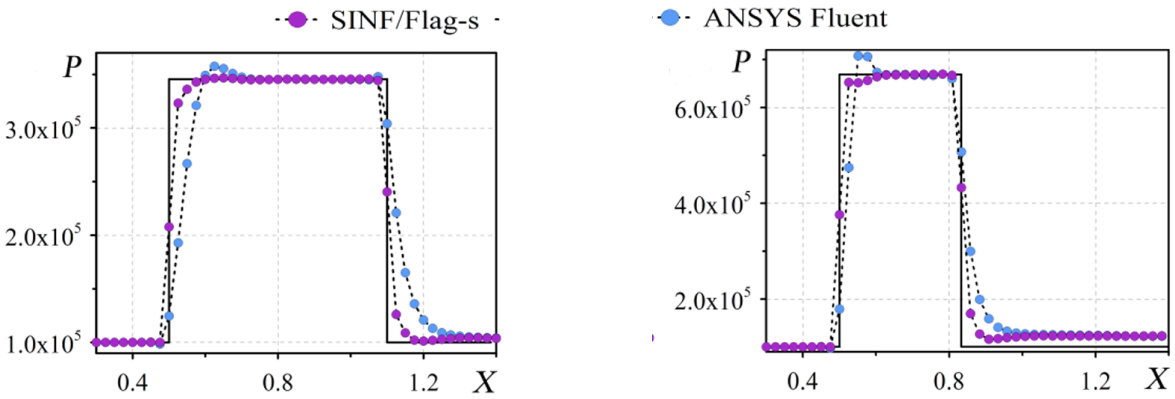

(a) M = 3 and a $\theta = 16.7°$ ramp

(b) M = 3 and a $\theta = 30.9°$ ramp

Figure 13: Kolesnik and Smirnov Pressure Distributions

The observed trends correspond with my own pressure ratio measurements across the oblique shock. Specifically, I found pressure ratios of 3.12 and 6.68 for the respective cases. This indicates that not only do the mach contours and pressure contours (as depicted in the additional figures under the appendix) align visually, but the pressure ratios experienced across the shock are consistent with both each other and theoretical expectations. This consistency is illustrated in the figure below for angles of $\theta = 16.7°$ and $\theta = 30.9°$ using my own solver.

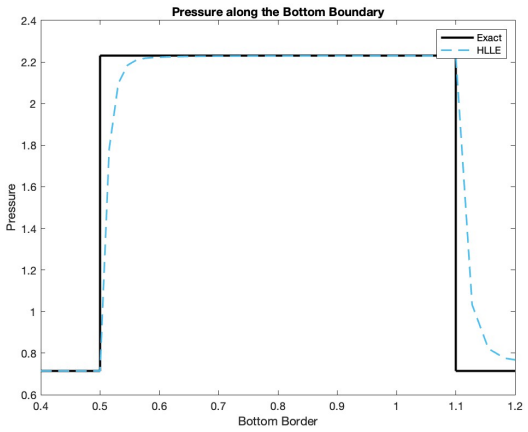

(a) M = 3 and a $\theta = 16.7°$ ramp

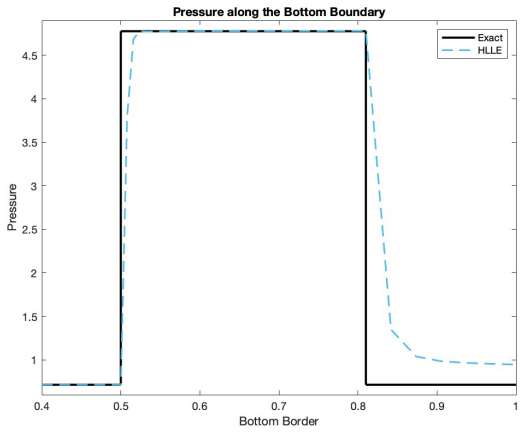

(b) M = 3 and a $\theta = 30.9°$ ramp

Figure 14: Pressure Distributions using my HLLE solver

I have greater confidence in my own solver's numerical results when they correlate with those of a commercial solver, such as ANSYS, and show similar trends. In both solvers, a clear deviation from theory was observed immediately following the expansion fan or turning of the flow aft of the ramp. The solvers provided a slightly higher pressure than expected in the "ideal case". Additionally, both solvers deviated at the base of the ramp, indicating the need for a better solver in real-world applications. However, as they follow the same trends, this is ultimately a positive sign for my numerical simulation. To ensure that our solvers match, it would be beneficial to compare pressure ratios across the entire domain, especially for pressures off of the boundary walls. Unfortunately, these plots are not currently provided in the Kolesnik paper, so this is not feasible at the moment.

7 Conclusion

This study aimed to investigate the behavior of supersonic flow undergoing ramp compression in a 2D wind tunnel, based on simplifying assumptions such as 2D flow, inviscid, and compressible conditions. The accuracy of this approach was demonstrated by comparing the results with existing literature and analytical solutions. The finite volume method was employed, using Godunov's method with Roe's approximate Riemann solver, as well as HLLE scheme to approximate the numerical fluxes across the finite control volumes. While the division of control volumes into triangular shapes may seem laborious, it was found to be an effective way to increase the discretization of the domain and improve solution accuracy, particularly for low accuracy solvers like Roe. As expected, HLLE outperformed Roe in terms of accuracy in both post-shock pressure ratios and mach contours. Future work could utilize the HLLE+ flux method to develop a more comprehensive solver with MUSCL or WENO. Moreover, the HLLE solver could be further applied to more complex-shaped geometries and higher-order time discretization schemes for more accurate results.

References

[1] Burning, Nichols, R. H., & Tramel, R. W. (2009). *Addition of Improved Shock-Capturing Schemes to OVERFLOW 2.1.*

[2] DeBonis, J. R. (2011, January 06). Mach 2.0, 15 degree wedge. Retrieved March 16, 2023, from https://www.grc.nasa.gov/WWW/wind/valid/wedgeM2/wedgeM2.html

[3] Kolesnik, & Smirnov, E. M. (2018). Some aspects of numerical modeling of inviscid supersonic flow in a duct with a central wedge. *Journal of Physics. Conference Series*, 1038(1), 12133–. https://doi.org/10.1088/1742-6596/1038/1/012133

[4] S. Park, C. Lee, & K. Kang. (n.d.). Navier-Stokes analysis of a supersonic flow over moving compression ramp. In *39th Aerospace Sciences Meeting and Exhibit. https://doi.org/10.2514/6.2001-568*

[5] Toro. (2009). *Riemann solvers and numerical methods for fluid dynamics*: *a practical introduction / Eleuterio F. Toro. (3rd ed.)*. Springer.

[6] Sergei Konstantinovich Godunov. "A difference method for numerical calculation of discontinuous solutions of the equations of hydrodynamics". In: *Matematicheskii Sbornik* 89.3 (1959), pp. 271–306.

[7] LeVeque. (2002). *Finite Volume Methods for Hyperbolic Problems.* Cambridge University Press.

[8] Park, S.-H. and Kwon, J., "An Improved HLLE Method for Hypersonic Viscous Flows," AIAA-2001-2633, June 2001.

8 Appendices

8.1 Supplementary Figures

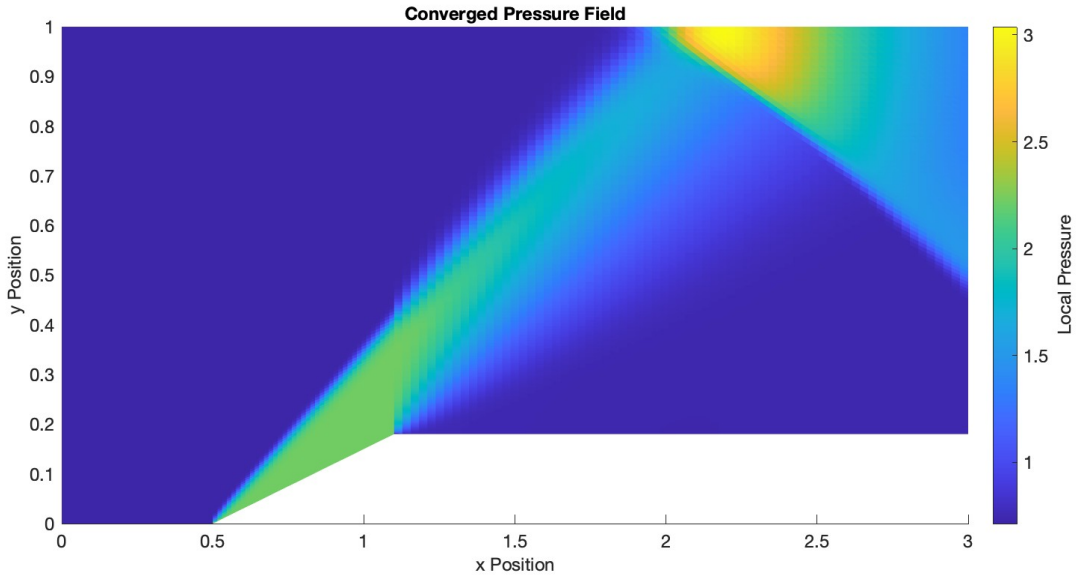

Figure 15: Pressure contour for $M = 3$ and atand $= 0.3$

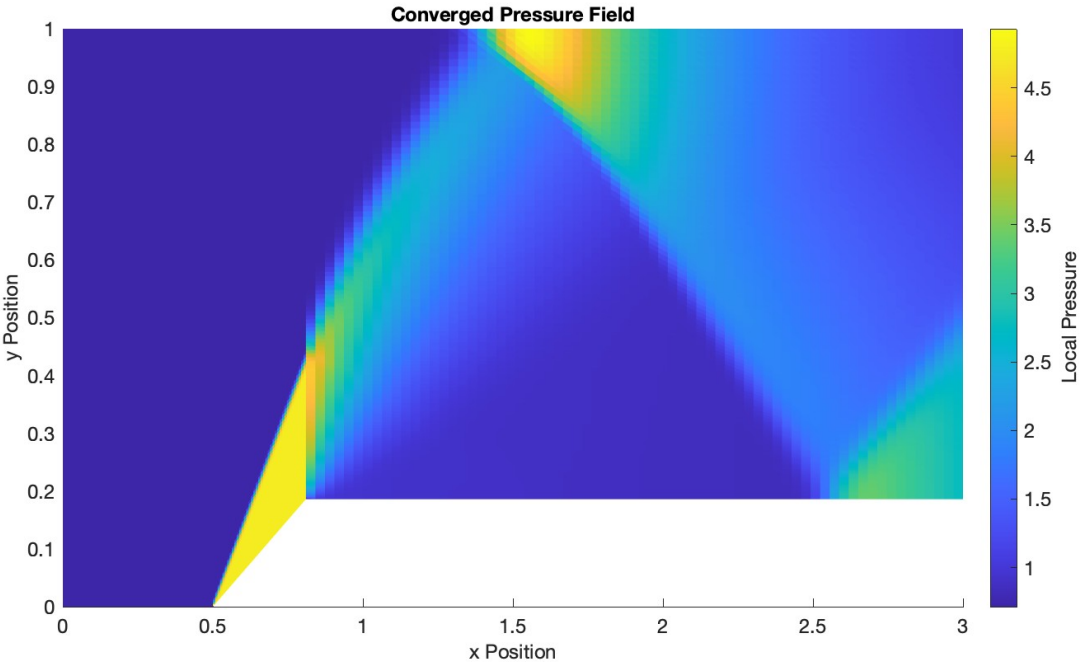

Figure 16: Pressure contour for $M = 3$ and atand $= 0.6$